

DESIGN AND FABRICATION OF A QUAD-BAND BANDPASS FILTER USING MULTI-LAYERED SIR STRUCTURE

R.-Y. Yang

Department of Materials Engineering
National Pingtung University of Science and Technology
No. 1, Syuefu Rd., Neipu Township, Pingtung County 91201, Taiwan

C.-Y. Hung

Department of Electronics Engineering and Computer Science
Tung-Fang Design University
No. 110, Tungfung Rd., Hunei Township
Kaohsiung County 82941, Taiwan

J.-S. Lin

Department of Materials Engineering
National Pingtung University of Science and Technology
No. 1, Syuefu Rd., Neipu Township, Pingtung County 91201, Taiwan

Abstract—In this paper, design and fabrication of a quad-band microstrip bandpass filter (BPF) using multi-layered stepped impedance resonators (SIRs) structure is proposed. One pair of SIR on the top layer is designed to operate at the 1st and 3rd passbands (1.56/3.57 GHz), and the other pair is at 2nd and 4th passbands (2.42/5.23 GHz) by tuning the impedance and length ratios of the SIRs. In order to find the desired coupling location between the SIRs located on different layers and the input/output (I/O) lines, the voltage, current and power wave on the I/O lines are analyzed. It is verified that the proposed quad-band filter has good passband performances with an excellent isolation between adjacent bands for GPS, WLAN, and WiMAX applications.

1. INTRODUCTION

Recently, multi-service wireless communication systems, such as the applications of global positioning system (GPS), wireless local area network (WLAN), and IEEE 802.16 worldwide interoperability for microwave access (WiMAX) are well developed [1–4]. Therefore, multi-band bandpass filters (BPFs) have gained much attention due to the key component in the RF front end. Methods to design the dual-band BPF are well developed and reported [5–8, 15]. However, only a few methods for quad-band bandpass filters have been reported till now [9–12].

Negative-refractive-index transmission-line (NRI-TL) metamaterials are used to realize a quad-band BPF [9], by varying the parameters of the NRI-TL. Coplanar waveguide (CPW)-fed dual-mode double-square-ring resonators were used for the quad-band filter [10], by tuning the perimeter ratio of the square rings. However, the parameters of the above design are too complex, and the circuit sizes are large. Half-wavelength coupled uniform impedance resonators (UIRs) and defected ground structures (DGSs) on the ceramic substrate using a screen-printing technique were used for a quad-band filter [11]. However, the use of DGSs would disturb the signal integrity on the ground plane for package, and the design freedom would be limited. The challenges for circuit designers to design a quad-band BPF are to achieve compact size and good passband selectivity simultaneously. As known, conventional stepped impedance resonators (SIRs) can shift the higher order resonant mode to the desired frequency, thus the SIRs are suitable for a wide stopband, an ultra-wide band (UWB) or a multi-band use [12].

In this paper, we propose a new quad-band filter using multi-layered SIRs structure, designed at 1.56/2.42/3.57/5.23 GHz for the combination of GPS (1.575 GHz), WLAN (2.4/5.2 GHz), and WiMAX (3.5 GHz) applications. The quad-passbands are determined by properly tuning the dimension of the SIRs. It is verified that the proposed BPF has a compact circuit size and good passband selectivity due to use of multi-layered structure. In the first steps, the resonant modes of the SIRs are analyzed and the dimension selection of the SIRs is discussed. In the second steps, the voltage, current and power wave on the input/output (I/O) lines are analyzed in order to fine the desired coupling location between the SIRs located on different layers and I/O lines. Finally, the designed BPF is fabricated and measured.

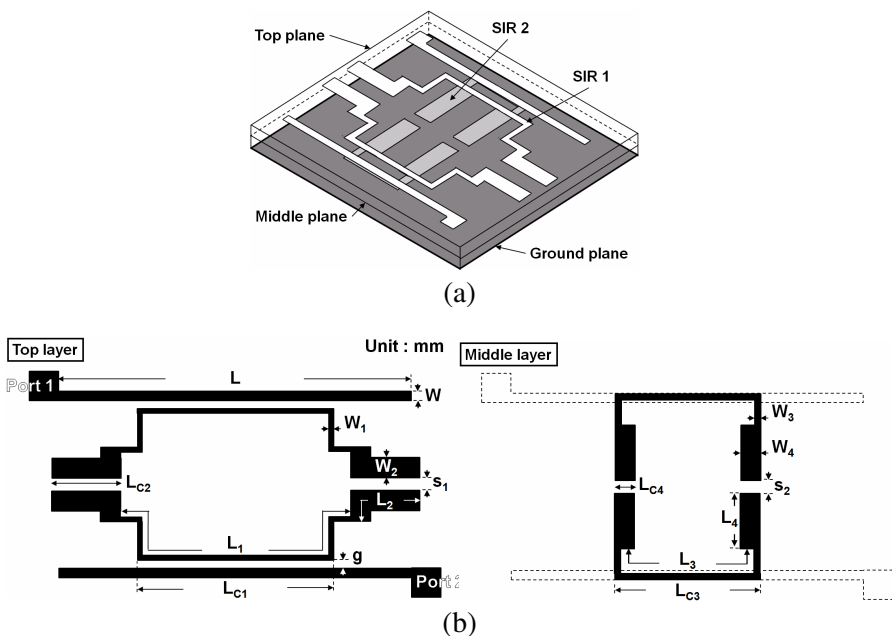


Figure 1. (a) A three-dimensional view of the quad-band BPF. (b) Two-dimensional views of the top and middle planes.

2. DESIGN PROCEDURES

The three dimensional view of the proposed quad-band BPF is shown in Figure 1(a), and the configuration of the top and middle planes for the SIRs is shown in Figure 1(b). In this structure, the I/O line is on the top layer. The pair of the SIR on the top layer is designed for the first and third passbands (1.56/3.57 GHz), and the pair of the SIR on the middle layer is designed for the second and fourth passbands (2.42/5.23 GHz). The multilayered substrate is constructed by stacking two Duroid 5880 substrate with a dielectric constant ϵ_r of 2.2, and a loss tangent of 0.0009.

To obtain the quad-band response, higher order modes of the SIR shall be discussed and shifted to the desired frequencies. Figure 2(a) shows the configuration of the SIR. θ_1 and θ_2 are the electrical lengths of the high impedance Z_1 and the low impedance Z_2 , respectively. The impedance ratio (K) and length ratio (α) are defined as $K = Z_2/Z_1$ and $\alpha = 2\theta_2/\theta_t = \theta_2/(\theta_1 + \theta_2)$, respectively. The input admittance Y_{in} of the SIR can be derived as [13–15]

$$Y_{in} = \frac{2(K \tan \theta_1 + \tan \theta_2) \cdot (K - \tan \theta_1 \cdot \tan \theta_2)}{K(1 - \tan^2 \theta_1) \cdot (1 - \tan^2 \theta_2) - 2(1 + K^2) \cdot \tan \theta_1 \cdot \tan \theta_2} \quad (1)$$

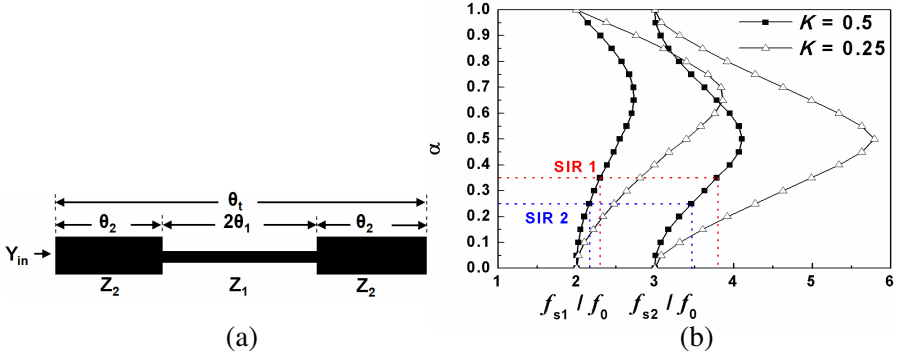


Figure 2. (a) Schematic of the stepped-impedance resonator, (b) second and third order resonant modes versus fundamental resonant modes (f_{s1}/f_0 and f_{s2}/f_0) as function of the length ratio α and impedance ratio $K = 0.5$, and 0.25 .

It is known that the SIR can resonate when $Y_{in} = 0$. Substituting α into Equation (1), the various resonant modes can be tuned based on the specific K and α , as shown in Figure 2(b).

In this example, the K/α values are selected as $0.5/0.5$ and $0.35/0.25$ for the pair of SIR on the top (SIR 1) and middle layer (SIR 2), respectively. For practice fabrication consideration, the half-wavelength SIR 1/SIR 2 has the high-impedance, $Z_1 = 158/107 \Omega$ to have a line section with a strip width of $0.4/0.6$ mm (W_1/W_3) and the low-impedance, $Z_2 = 79/53 \Omega$ to have a line sections with a strip width of $2.27/2.2$ mm (W_2/W_4). The location of the resonators versus I/O microstrip lines plays an important role in the performance of the filter and will determine the cross-coupling effect of the architecture. Therefore, the coupling properties of SIR 1 and SIR 2 will be discussed on the top and middle planes individually for the optimal quad-band performance.

In order to fine the desired coupling location between the SIRs located on different layers and I/O lines, the electromagnetic (EM) properties on the I/O open-end transmission line are simulated. For SIR 1 on the top layer, the I/O terminated lines have characteristic impedance $Z_0 = 117 \Omega$ ($W = 1$ mm) and length $L = 45.29$ mm (around $0.32\lambda_g$, where λ_g is the guided wavelength at the 1.575 GHz). Based on the transmission line theory, voltages, currents, and impedances are varied in magnitude and phase over the length for plane wave propagation [16]. Once the terminated lines assume as lossless, the voltages, currents, and impedances on the open-ended line are

expressed as

$$V(\ell) = 2V_0^+ \cos \beta z \tag{2}$$

$$I(\ell) = \frac{-2jV_0^+}{Z_0} \sin \beta z \tag{3}$$

$$Z_{in} = -jZ_0 \cot \beta z \tag{4}$$

where β represents the phase constant of the traveling waves.

According to (2), (3), and (4), the propagation of the electromagnetic waves on the open-ended microstrip lines can be

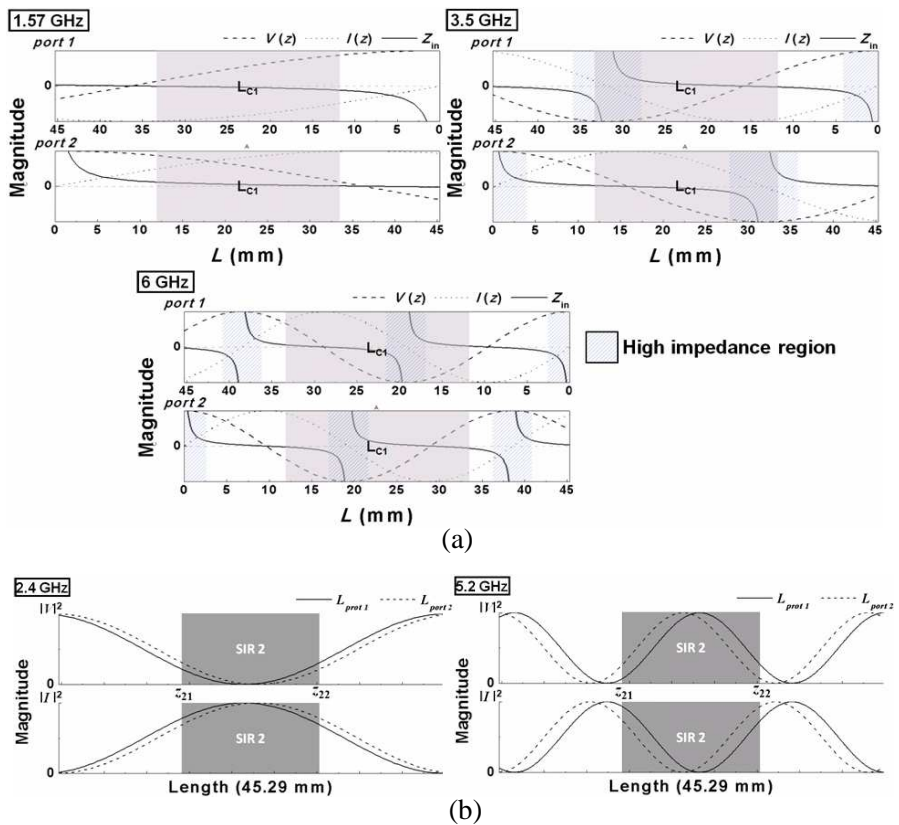


Figure 3. (a) Normalized voltages, currents, and impedances along the I/O terminated line in an open circuit at 1.57, 3.5, and 6 GHz for SIR 1, and (b) the distribution of normalized $|V|^2$ and $|I|^2$ over the I/O microstrip lines at 2.4 and 5.2 GHz for SIR 2. The larger light gray rectangle marks the coupling region of SIR 1, and the smaller heavy gray one marks the coupling region L_{C3} of SIR 2.

computed and simulated [17]. The normalized voltages, currents, and impedances at the first, second, and third resonant frequencies, 1.57, 3.5, and 6 GHz, along the open-ended terminated lines are shown in Figure 3(a). The desired fundamental and third passbands for GPS and WiMAX applications can be achieved by impedance and electrical length ratio of the SIR 1. When resonating, there is a weakest coupling point at $n \times \lambda/2$, and $n = 1, 2, 3, \dots$, λ is the wavelength at resonant frequency, to create a high impedance region around itself on the open-end I/O lines. However, an unwanted third harmonic excites at 6 GHz and will regard the performance significantly for a quad-band performance. In order to overcome this issue, the coupling region L_{C1} must be designed to cover the high impedance region, and the position of SIR 1 versus I/O lines should be selected properly.

Figure 4(a) depicts that port 1 and port 2 lines are alone shifted left and right respectively in views of the coupling region L_{C1} of SIR 1 being 20.8 mm (about half-wavelength at 6 GHz). As the center of $L_{C1} = 20.8$ mm locating at 17.65 mm from the terminations of two I/O lines (i.e., the first weak coupling point), the coupling energy between I/O lines and SIR 1 cannot transfer each other completely because the high impedance region is covered with L_{C1} at 6 GHz. Therefore, the second and third harmonics are suppressed as shown in Figure 4(b). Furthermore, the location of SIR 1 can be varied slightly at the middle of I/O lines for a compact size by displacing 5 mm of port 1/port 2 line right/left. Consequentially, L_{C1} is estimated to range from 12.2 mm of port 1 to 33.1 mm of port 2 for a better performance as the centers of SIR 1 and I/O lines are collinear.

Besides, the optimal coupling region L_{C3} of SIR 2 on the middle layer can be obtained based on prior research [15] for dual-band

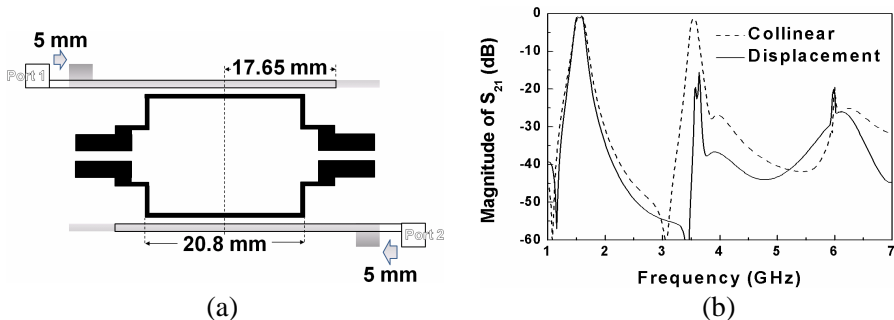


Figure 4. (a) The configuration with a displacement = 17.65 mm from the center of $L_{C1} = 20.8$ mm to the I/O line end on the top layer. (b) The simulated frequency responses of (a) and the optimal result with collinear centers of SIR 1 and I/O lines.

performance without the spurious responses. It is known that the external quality factor is proportional to the coupling coefficient inversely. In views of the performance, the coupling region L_{C3} (i.e., heavy gray portions in Figure 3(b)) of the SIR 2 versus I/O microstrip lines is selected by optimizing the coupling coefficient magnitude. Figure 3(b) shows the absolute square value of the normalized voltages and currents over the I/O microstrip lines at 2.4 and 5.2 GHz on the middle layer by using (2) and (3). The electric and magnetic coupling coefficients for the defined coupling regions L_{C3} of SIR 2, i.e., between z_{21} and z_{22} , can be expressed:

$$|k_e| = C \times \int_{z_{21}}^{z_{22}} |V(\ell)|^2 d\ell = C \times \int_{z_{21}}^{z_{22}} (\cos \beta\ell)^2 d\ell \quad (5)$$

and

$$|k_m| = C \times \int_{z_{21}}^{z_{22}} |I(\ell)|^2 d\ell = C \times \int_{z_{21}}^{z_{22}} (\sin \beta\ell)^2 d\ell, \quad (6)$$

where C is a positive constant. Therefore, we can recommend the magnitude of the coupling coefficient in the defined coupling region L_{C3} by integrating $|V|^2$ and $|I|^2$ form z_{21} to z_{22} in Figure 3(b). Since the electric and magnetic coupling coefficients are out of phase, the total coupling coefficient has a minimum integration when the coupling region is at the middle of L . Besides, a shorter coupling region L_{C1} causes a larger external quality factor but a degraded coupling strength. Therefore, we can estimate the proper coupling L_{C3} to the required performance. In this example, L_{C3} can be decided as 16.4 mm when the center of SIR 2 is set at the middle of L on the middle layer. Figure 5 shows the current distributions of the proposed filter at 1.56, 2.42, 3.57 and 5.23 GHz. It is verified that the EM waves are transmitted in the filter from port 1 to port 2.

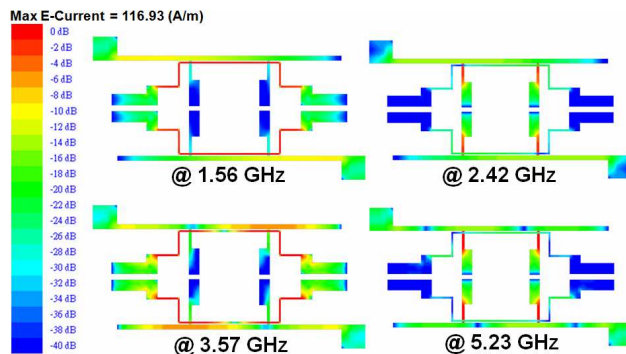


Figure 5. Current distributions of the proposed filter at 1.56, 2.42, 3.57, and 5.23 GHz.

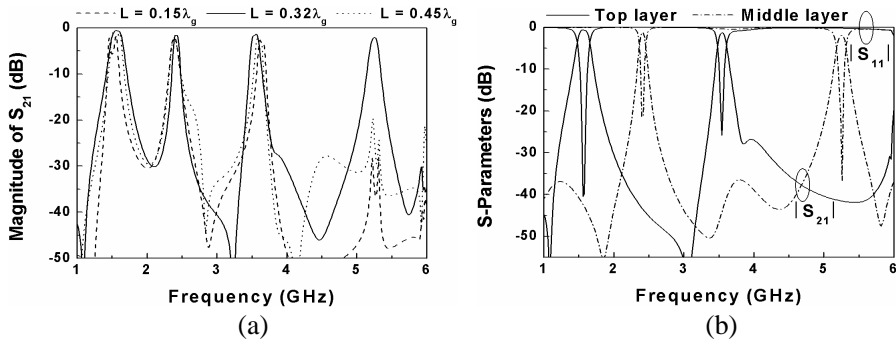


Figure 6. (a) The simulated frequency responses for the proposed quad-band BPF with various I/O microstrip line lengths. (b) SIR 1 on the top and SIR 2 middle layers individually.

Figure 6(a) shows the simulated frequency response of the proposed filter with various lengths ($0.15\lambda_g$, $0.32\lambda_g$, and $0.45\lambda_g$) of the I/O microstrip lines. It is clearly observed that different lengths of the I/O lines cause different performances of the filter with the same resonators. Thus, once the strip length is altered, the EM field on the line will be varied, and the coupling region has to be redefined further in the new length. Furthermore, it should be noted that two SIR pairs overlap vertically or do not disturb the signal integrity on the ground plane. Figure 6(c) shows the stacked simulated frequency responses of SIR 1 on the top layer and SIR 2 on the middle layer individually. The simulated insertion losses $|S_{21}|$ are 0.65/1.3/1.3/1.9 dB, for the four passbands of the two layers. Compared with the simulated results of the multi-layered structure ($|S_{21}| = 0.65/1.65/1.37/1.98$ dB), the deviation caused by the two SIRs sharing the coupling energy of I/O lines over the overlapped region simultaneously is small enough which can be ignored. Two SIRs may be separated by different vertical axes to avoid the disturbance, but the overall size will be increased. Consequently, there is a spacing of 3.6 mm between SIR1 and SIR 2 in this example.

3. RESULTS AND DISCUSSION

Based on the above discussion, the optimized structural parameters of the designed filter example are $L_1 = 38.76$ mm, $L_2 = 11.03$ mm, $L_{C1} = 20.8$ mm, $L_{C2} = 9.33$ mm, $L_3 = 25.05$ mm, $L_4 = 5.27$ mm, $L_{C3} = 16.4$ mm, $L_{C4} = 2.2$ mm, $s_1 = 1.2$ mm, $s_2 = 0.9$ mm, $g = 0.2$ mm, and two feed ports are 4.84 mm wide, corresponding to a 50Ω microstrip. The designed filter was fabricated using the carving

machine, and the top and middle layers are stacked together. The sample was measured by an HP8510C Network Analyzer. The whole size of the fabricated filter is $45.29 \text{ mm} \times 21.29 \text{ mm}$, i.e., approximately $0.32\lambda_g$ by $0.15\lambda_g$, where λ_g is the guided wavelength at the center frequency of the fundamental passband at 1.574 GHz.

Figure 7(a) shows the photograph of the fabricated layout. Figure 7(b) shows the simulated and measured results. The fabricated

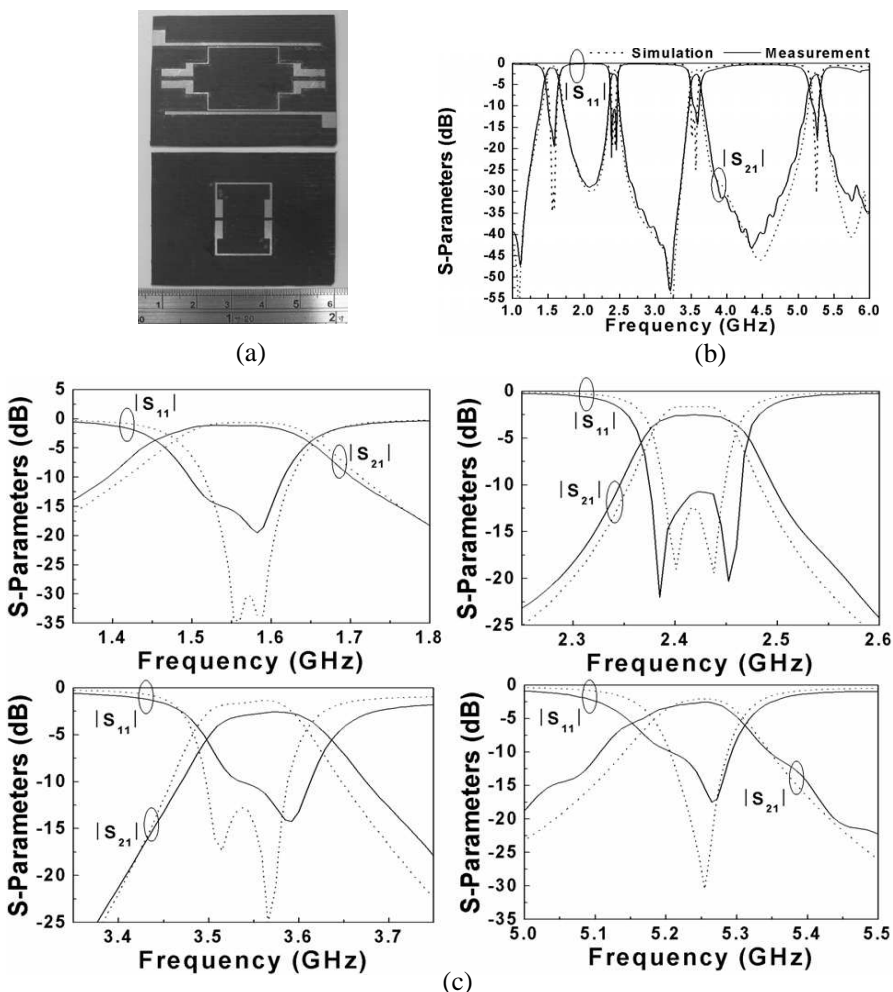


Figure 7. (a) Picture, (b) simulated and measured frequency response of the designed quad-band BPF, and (c) the enlarged views of the simulated and measured frequency responses at four passbands, respectively.

Table 1. The comparison with other quad-band filters. (λ_g is the guided wavelength at the center frequency of the fundamental passband.)

	[9]	[10]	Proposed filter
Substrate height (mm)/ ϵ_r	PCB 1.27/10.2	PCB 1.57/3	PCB 1.574/2.2
Center frequency at four passbands (GHz)	0.87/1.055/ 1.775/2	0.9/1.26/ 1.89/2.29	1.56/2.42/ 3.57/5.23
Return loss (dB)	31/29/ 28/23	23/23/ 25/30	16/12/ 13/12.5
Insertion loss (dB)	0.94/1.1/ 0.73/1.8	2.2/2.1/ 1.4/0.9	1.1/2.5/ 2.5/2.8
3-dB FBW (%)	2.8/2.8/ 3.9/6.5	6.7/5.4/ 12/15.3	13/4.3/ 4/2.9
Circuit Size (mm ²) ($\lambda_g \times \lambda_g$)	1148 (0.4 \times 0.2)	2401 (0.3 \times 0.3)	964 (0.32 \times 0.15)

filter has measured center frequencies at 1.56/2.42/3.57/5.23 GHz, the 3-dB fractional bandwidth (FBW) of 13/4.3/4/2.9%, the insertion loss ($|S_{21}|$) of 1.1/2.5/2.5/2.8 dB and the return loss ($|S_{11}|$) of 16/12/13/12.5 dB, as shown in Figure 7(c). Two transmission zeros can be obtained at 1.11 and 3.21 GHz, thus the band isolations are 30 dB, 50 dB and 45 dB between adjacent passbands. The measured results actually verify the possibility of the proposed design concept. The proposed quad-band filter with multi-layered structure shows compact size and good passband selectivity comparing with other reported structures [9, 10], as shown in Table 1. The filter has slightly higher insertion losses than others. It is believed that the stacked substrates have an air gap due to home-made fabrication deviation, causing higher insertion losses and can be improved when using more precise technology in the factory.

4. CONCLUSIONS

We have proposed a new quad-band filter using multi-layered SIRs structure, designed at 1.56/2.42/3.57/5.23 GHz for the combination of GPS (1.575 GHz), WLAN (2.4/5.2 GHz), and WiMAX (3.5 GHz)

applications. The quad-passbands are obtained by properly tuning the dimension of the SIRs. The voltage, current, and power wave on the I/O lines are analyzed to find the desired coupling location between the SIRs located on different layers and the input I/output O lines. The measured results for four passbands have the 3-dB fractional bandwidth (FBW) of 13/4.3/4/2.9%, the insertion loss ($|S_{21}|$) of 1.1/2.5/2.5/2.8 dB and the return loss ($|S_{11}|$) of 16/12/13/12.5 dB, respectively. Moreover, the proposed filter has a compact circuit size and good passband selectivity due to the use of multi-layered structure, compared to the other reported structures.

ACKNOWLEDGMENT

Financial support of this study by the National Science Council of the Republic of China under grant No. NSC 99-2221-E-272-007 is greatly appreciated.

REFERENCES

1. Soltani, S., M.-N. Azarmanesh, E. Valikhanloo, and P. Lotfi, "Design of a simple single-feed dual-orthogonal-linearly-polarized slot antenna for concurrent 3.5 GHz WiMAX and 5 GHz WLAN access point," *Journal of Electromagnetic Waves and Applications*, Vol. 24, No. 13, 1741–1750, 2010.
2. Mahatthanajatuphat, C., S. Saleekaw, P. Akkaraekthalin, and M. Krairiksh, "A rhombic patch monopole antenna with modified Minkowski fractal geometry for UMTS, WLAN, and mobile WiMAX application," *Progress In Electromagnetics Research*, Vol. 89, 57–74, 2009.
3. Zhao, Q., S.-X. Gong, W. Jiang, B. Yang, and J. Xie, "Compact wide-slot tri-band antenna for WLAN/WiMAX applications," *Progress In Electromagnetics Research Letters*, Vol. 18, 9–18, 2010.
4. Chang, T. N., G. Y. Shen, and J. M. Lin, "CPW-fed antenna covering WiMAX 2.5/3.5/5.7 GHz bands," *Journal of Electromagnetic Waves and Applications*, Vol. 24, Nos. 2–3, 189–197, 2010.
5. Weng, M. H., C. H. Kao, and Y. C. Chang, "A compact dual-band bandpass filter with high band selectivity using cross-coupled asymmetric SIRs for WLANs," *Journal of Electromagnetic Waves and Applications*, Vol. 24, Nos. 2–3, 161–168, 2010.
6. Lee, C.-H., I.-C. Wang, and C.-I. G. Hsu, "Dual-band balanced BPF using $\lambda/4$ stepped-impedance resonators and folded feed

- lines,” *Journal of Electromagnetic Waves and Applications*, Vol. 23, Nos. 17–18, 2441–2449, 2009.
7. Weng, M.-H., S.-K. Liu, H.-W. Wu, and C.-H. Hung, “A dual-band bandpass filter having wide and narrow bands simultaneously using multilayered stepped impedance resonators,” *Progress In Electromagnetics Research Letters*, Vol. 13, 139–147, 2010.
 8. Hu, X., Q. Zhang, and S. He, “Compact dual-band rejection filter based on complementary meander line split ring resonator,” *Progress In Electromagnetics Research Letters*, Vol. 8, 181–190, 2009.
 9. Studniberg, M. and G. V. Eleftheriades, “A quad-band bandpass filter using negative-refractive-index transmission-line (NRI-TL) metamaterials,” *IEEE Antennas and Propagation Society International Symposium*, 4961–4964, 2007.
 10. Liu, J. C., J. W. Wang, B. H. Zeng, and D. C. Chan, “CPW-fed dual-mode double-square-ring resonators for quad-band filters,” *IEEE Microw. Wireless Compon. Lett.*, Vol. 20, 142–144, 2010.
 11. Cheng, C. C. and C. F. Yang, “Develop quad-band (1.57/2.45/3.5/5.2 GHz) bandpass filters on the ceramic substrate,” *IEEE Microw. Wireless Compon. Lett.*, Vol. 20, 594–596, 2010.
 12. Hsu, K. W. and W. H. Tu, “Design of a novel four-band microstrip bandpass filter using double-layered substrate,” *IEEE Microwave Symposium Digest*, 1041–1044, 2009.
 13. Chang, Y. C., C. H. Kao, M. H. Weng, and R. Y. Yang, “Design of the compact wideband bandpass filter with low loss, high selectivity and wide stopband,” *IEEE Microw. Wireless Compon. Lett.*, Vol. 18, 770–772, 2008.
 14. Yang, R.-Y., C.-Y. Hung, J.-S. Lin, and Y.-K. Yang, “A simple method to design a compact triple-passband filter using novel coupling scheme and multi-layered substrate,” *Journal of Electromagnetic Waves and Applications*, Vol. 25, Nos. 2–3, 443–453, 2011.
 15. Yang, R.-Y., C.-Y. Hung, and J.-S. Lin, “A dual-band bandpass filter with an enhanced second passband performance using modifiable coupling,” *Journal of Electromagnetic Waves and Applications*, Vol. 25, Nos. 2–3, 305–314, 2011.
 16. Pozar, D. M., *Microwave Engineering*, 2nd edition, Wiley, New York, 1998.
 17. *IE3D Simulator*, Zeland Software, Inc., 2002.